Hybrid lumped/distributed parameter model for treating the vessel lower head ablation by corium during a LWR severe accident

M. Peybernes, R. Letellier, L. Viot, A. Drouillet, L. Saas

NENE 2018
September 10-13
PORTOROŽ
SLOVENIA
27th International Conference Nuclear Energy for New Europe

Hybrid lumped/distributed parameter model for treating the vessel lower head ablation by corium during a LWR severe accident

M. Peybernes
CEA, DEN, DTN/SMTA/LMAG, Cadarache
F-13108 Saint Paul-lez-Durance, France
mathieu.peybernes@cea.fr

R. Le Tellier, L. Viot, A. Drouillet, L. Saas
CEA, DEN, DTN/SMTA/LMAG, Cadarache
F-13108 Saint Paul-lez-Durance, France
romain.le-tellier@cea.fr, louis.viot@cea.fr, adrien.drouillet@cea.fr, laurent.saas@cea.fr

ABSTRACT

Within the context of Severe Accident for Light Water Reactors, the studies of in-vessel corium behavior and associated risk of vessel failure are matters of prime interest. The corium heat flux at the pool interface can lead to the ablation of the steel vessel wall. The ablation kinetics is of prime interest when considering the possible formation of a "thin" metal phase on the top of the pool and the potential vessel failure at that point due to heat flux concentration, in particular when evaluating the chances of success of in-vessel retention (IVR) strategy. In the framework of so-called severe accident codes where fast-running models are used, standard models based on a 2D meshing of the wall can become impractical in particular when a too thin metal phase appears. Thus, this paper is focused on a simplified yet accurate modelling of the wall heating and ablation. It is based on a 1D axial meshing of the wall. For each wall mesh, radial heat fluxes at the wall internal and external boundaries are calculated following a lumped parameter modelling approach while the axial heat fluxes are approximated by a first-order finite difference formula. This model is validated against reference 2D solutions of the heat equation on pure conduction cases starting from a typical in-vessel configuration and constructed from nondimensionalization considerations. Finally, this model is applied to in-vessel corium transient calculations under IVR conditions.

1 INTRODUCTION

The knowledge of in-vessel corium behavior and associated risk of vessel failure are matters of prime interest within the framework of Severe Accident studies for Light Water Reactors (LWRs). Core meltdown during a severe accident can result into formation of a corium pool (oxidic and metallic liquid materials) at the bottom of the reactor vessel.

The volumetric heat generation associated with decay heat induces natural convection in the pool that, combined with phase segregation effects, determines the heat flux distribution at the pool interface. In particular, along the lateral boundary, this heat flux leads to the ablation

of the steel vessel wall. The ablation kinetics of the vessel wall is of prime interest when considering the possible formation of a "thin" metal phase on the top of the pool and the potential vessel failure at that point due to heat flux concentration (the so-called focusing effect) [1, 2] As a consequence, when evaluating the chances of success of in-vessel retention (IVR), the transient ablation of the vessel wall has to be carefully modeled. On one hand, the axial conduction within the wall can only be neglected during the first stage of ablation transients and has to be taken into account when long-term retention of the corium is to be evaluated. On the other hand, when considering a stratified corium pool, the axial meshing of the wall should be fine enough to avoid any smearing of the heat flux associated with the top metal phase. In the general case, as the position of this layer changes with time, a fine mesh is required on a large part of the wall. Consequently, in the framework of so-called severe accident codes where fast-running models are used, standard models based on a 2D meshing of the wall (and, for instance a source-based enthalpy method for the Stefan problem [3]) can become impractical.

In the frame of the PROCOR software platform development [4], so far, the modeling effort in PROCOR has been mainly put on the stratified pool and the associated stratification kinetics [5] in such a way that the vessel wall discretized by 1D axial meshing was treated in crude way by neglecting the axial conduction as in [6] in such a way that the one-phase Stefan problems associated with the different meshes are decoupled. The system of ordinary differential equations (ODEs) associated with the lumped mass and energy conservation equations is then closed by a radial quadratic temperature profile assumption that was proven accurate in the 1D case in [7].

This paper discusses a possible improvement of this model where the axial conduction is taken into account by approximating the axial heat fluxes by a first-order finite difference formula while keeping the same ODE formulation.

Section 2 summarizes the existing lumped parameter modeling of the wall conduction in PROCOR along with the proposed hybrid treatment of the axial conduction ; in addition, a finite-element discretization of the 2D problem is also presented as it will be used for generating a reference solution in the numerical tests presented in Section 3. These test cases without ablation are based on a typical in-vessel configuration and constructed from nondimensionalization considerations. Finally, the enhanced PROCOR model is tested on an in-vessel corium transient calculation under IVR conditions where the impact of axial conduction is discussed (see Section 4).

2 CONDUCTION MODELING

The 2D vessel domain is denoted by Ω_V. The physical properties of the vessel are: $\mathbf{T_V}$ the temperature, ρ_V the density, λ_V the thermal conductivity and $C_{p,V}$ the specific heat capacity. We note γ_{ext} the boundary part of domain Ω_V where the temperature $\mathbf{T}_{ext}$ is imposed and γ_{in} the boundary part with an imposed heat flux $\boldsymbol{\phi}_{in}$ (which can be partly null for the adiabatic parts of the domain boundary).

2.1 Finite element 2D discretization

In the vessel, the temperature $\mathbf{T}_V$ is governed by the heat conduction equation:

$$\rho_V C_{p,V} \frac{d\mathbf{T}_V}{dt}(\mathbf{r},t) - \lambda_V \Delta \mathbf{T}_V(\mathbf{r},t) = 0 \qquad \text{for } \mathbf{r} \in \Omega_V \tag{1}$$

$$-\lambda_V \nabla \mathbf{T}_V(\mathbf{r},t) = \boldsymbol{\phi}_{in}(\mathbf{r},t) \qquad \text{for } \mathbf{r} \in \gamma_{in} \tag{2}$$

$$\mathbf{T}_V(\mathbf{r},t) = \mathbf{T}_{ext}(\mathbf{r},t) \qquad \text{for } \mathbf{r} \in \gamma_{ext} \tag{3}$$

System of Eq. 1 to Eq. 3 are discretized using 2D linear finite elements $\mathbb{Q}_1$.

2.2 1D slab approximation

The vessel geometry is assumed to be *rectangular*. It is discretized in 1D along the axial direction of the vessel (denoted by the z-axis). The vessel mesh is described by N_{nodes} given nodes. The $N_{cells} = N_{nodes} - 1$ corresponding *rectangular* cells are denoted by C_j for $1 \leq j \leq N_{cells}$. For each cell, the radial direction is denoted by the x-axis. Its origin is chosen on boundary $\gamma_{in} \cap C_j$ while the external boundary $\gamma_{ext} \cap C_j$ is at $x = L$ (see Figure 1).

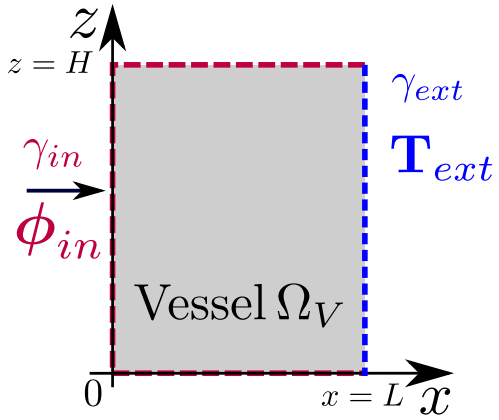

Figure 1: Notations for the vessel discretization

At each cell j, the 1D heat conduction problem given by equations Eq. 1 to Eq. 3 simplified under the 1D assumption is given by:

$$\rho_V C_{p,V} \frac{\partial T_{V,j}}{\partial t}(x,t) - \lambda_V \frac{\partial^2 T_{V,j}}{\partial x^2}(x,t) = 0 \qquad \text{for } x \in [0,L] \tag{4}$$

$$-\lambda_V \frac{\partial T_{V,j}}{\partial x}(x,t) = \phi_{in}(x,z,t) \qquad \text{for } (x,z) \in \gamma_{in} \tag{5}$$

$$T_{V,j}(x,t) = T_{ext}(x,z,t) \qquad \text{for } (x,z) \in \gamma_{ext} \tag{6}$$

with $T_{V,j}$ the axial temperature of cell j and where the axial conduction is not taken into account.

Then, the following averaged quantities are introduced:

$$m_{V,j}(t) = \rho_V V_j(t) \qquad \text{for} \quad 1 \leq j \leq N_{cells} \tag{7}$$

$$\overline{T}_{V,j}(t) = \frac{1}{L} \int_{x=0}^{x=L} T_{V,j}(x,t)\,\mathrm{d}x \qquad \text{for} \quad 1 \leq j \leq N_{cells} \tag{8}$$

$$\overline{\phi}_{j,in}(t) = -\lambda_V \frac{\partial T_{V,j}}{\partial x}(x=0,t) \qquad \text{for} \quad 1 \leq j \leq N_{cells} \tag{9}$$

$$\overline{\phi}_{j,ext}(t) = -\lambda_V \frac{\partial T_{V,j}}{\partial x}(x=L,t) \qquad \text{for} \quad 1 \leq j \leq N_{cells} \tag{10}$$

with V_j the volume of cell j.

In this way, the integral formulation of equation Eq. 4 leads to the macroscopic energy conservation equation for each cell j given by

$$C_{p,V}\, m_{V,j}(t) \frac{d\overline{T}_{V,j}}{dt}(t) = \left(\overline{\phi}_{j,in}(t) - \overline{\phi}_{j,ext}(t)\right) S_{j,rad} \tag{11}$$

with $S_{j,in} = S_{j,ext} = S_{j,rad}$ areas of surfaces $\gamma_{in} \cap C_j$ and $\gamma_{ext} \cap C_j$.

Obviously, for practical use, Eq. 11 needs proper closure laws for $\overline{\phi}_{j,in}$ and $\overline{\phi}_{j,ext}$ given by the relatively costly solving of Eq. 4. Proven accurate in 1D case in [7], a *lumped parameter* model, based on a radial quadratic temperature profile assumption, allows to bypass this numerical solving to directly deduce $\overline{\phi}_{j,in}$ and $\overline{\phi}_{j,ext}$.

2.3 Hybrid 1D/2D approximation

Because of the 1D slab approximation made at each cell j, the axial heat conduction between cells is neglected. As a remedy, axial heat fluxes are approximated using the average temperatures along the axial direction calculated by the 1D slab approximation along the radial direction, hence the *hybrid* 1D/2D approximation. Then, they are added to the macroscopic energy conservation Eq. 11.

At cell j, in between cells $j-1$ and $j+1$, axial heat fluxes through surfaces $C_{j-1} \cap C_j$ and $C_j \cap C_{j+1}$ with area $S_{j-1,j} = S_{j,j+1} = S_{j,ax}$ are given by[1]

$$\overline{\phi}_{j-1,j}(t) = -\frac{2\lambda_{V,j-1}\lambda_{V,j}}{\lambda_{V,j}e_{j-1} + \lambda_{V,j-1}e_j}\left(\overline{T}_{V,j-1} - \overline{T}_{V,j}\right) \tag{12}$$

$$\overline{\phi}_{j,j+1}(t) = -\frac{2\lambda_{V,j}\lambda_{V,j+1}}{\lambda_{V,j+1}e_j + \lambda_{V,j}e_{j+1}}\left(\overline{T}_{V,j} - \overline{T}_{V,j+1}\right) \tag{13}$$

$$\tag{14}$$

with e_{j-1}, e_j and e_{j+1} the respective heights of cells $j-1$, j and $j+1$. For

Then, the macroscopic energy conservation equation for the 1D/2D approximation is given by

$$C_{p,V}\, m_{V,j}(t)\frac{d\overline{T}_{V,j}}{dt}(t) = \left(\overline{\phi}_{j,in}(t) - \overline{\phi}_{j,ext}(t)\right) S_{j,rad} + \left(\overline{\phi}_{j-1,j}(t) - \overline{\phi}_{j,j+1}(t)\right) S_{j,ax} \tag{15}$$

with average radial heat fluxes given by Eqs. 9 and 10 under the quadratic temperature profile assumption.

3 BENCHMARKING ON PURE CONDUCTION TESTS

A nominal test case was constructed from a typical in-vessel configuration of interest for light water reactor severe accident analysis. In such a case, the maximum effect of axial conduction is expected to be at the top of the corium pool where, the flux onto the wall undergoes its largest discontinuity (the flux being zero above the pool when neglecting radiative heat trasfer to the vessel wall). The simple configuration reproducing such a flux discontinuity that has been used in these tests is depicted at Figure 1) with height $H = 0.5$ m, width $L = 0.15$ m and constant physical properties for the vessel wall. The initial uniform temperature of the vessel is set to 600 K. The fusion temperature of the vessel is set to an important value in such a way that ablation of the vessel never occurs during the transient. A constant temperature $T^{ext} = 400$ K is imposed at boundary γ_{ext} ($x = L$) of the vessel corresponding to the saturation temperature of water. The input heat flux ϕ^{in} imposed at boundary γ_{in} of the vessel is given by

$$\phi^{in} = \begin{cases} 0.5 & \text{MW/m}^2 \quad \text{if} \quad x = 0 \wedge z \leq H^{in} \\ 0 & \text{MW/m}^2 \quad \text{if} \quad x = 0 \wedge z > H^{in} \quad \text{or} \quad z = H \end{cases} \tag{16}$$

[1]For the sake of simplicity, the equations are presented for a rectangular geometry (*i.e.* not partially ablated) in such a way that the average temperature taken into account in the axial fluxes evaluations are directly the dependent variables of Eq. 11. In the general case, average temperatures over a restriction of C_j to $S_{j,j+1}$ is used for the evaluation of $\overline{\phi}_{j,j+1}$.

with $0 < H^{in} < H$ a parameter used for the sensitivity analysis.

To be more generic, the cases of study are selected with respect to a nondimensionalization of the heat conduction equations Eq. 1 to Eq. 3 solved in the vessel with a 2D rectangular geometry (with axis x and y) as in Figure 1.

The following notations are used for the nondimensionalization of these equations :

- the scaling quantities : time $t_\star$, width $x_\star$ and height $z_\star$, temperature $T_\star$ and heat flux $\phi_\star$.
- the dimensionless variables : $\tau = t/t_\star$, $\chi = x/x_\star$, $\zeta = z/z_\star$, $\chi^L = L/x_\star$, $\zeta^H = H/z_\star$, $\boldsymbol{\theta} = \boldsymbol{T}/T_\star$, $\boldsymbol{\theta}^{ext} = \boldsymbol{T}^{ext}/T_\star$, $\boldsymbol{\psi} = \boldsymbol{\phi}/\phi_\star$, $\boldsymbol{\psi}^{in} = \boldsymbol{\phi}^{in}/\phi_\star$
- the dimensionless numbers : the Fourier number $Fo = \frac{\lambda_V t_\star}{\rho_V C_{p,V} x_\star^2} = \frac{\alpha t_\star}{x_\star^2}$, the Biot number $Bi = \frac{\phi_\star x_\star}{\lambda_V T_\star}$, the width-height ratio $\Gamma = x_\star/z_\star$.

Then, the dimensionless heat conduction equation and associated dimensionless boundary conditions are given by

$$\frac{d\boldsymbol{\theta}_V}{d\tau} - Fo\left(\frac{\partial^2 \boldsymbol{\theta}_V}{\partial \chi^2} + \Gamma^2 \frac{\partial^2 \boldsymbol{\theta}_V}{\partial \zeta^2}\right) = 0 \quad \text{for} \quad (\chi, \zeta) \in \left[0, \chi^L\right] \times \left[0, \zeta^H\right] \tag{17}$$

$$\left[\frac{\partial \boldsymbol{\theta}_V}{\partial \chi}, \Gamma \frac{\partial \boldsymbol{\theta}_V}{\partial \zeta}\right]^T = -\frac{1}{Bi}\boldsymbol{\psi}^{in} \quad \text{for} \quad \chi = 0 \vee, \zeta = 0 \ \vee \ \zeta = \zeta^H \tag{18}$$

$$\boldsymbol{\theta}_V = \boldsymbol{\theta}^{ext} \quad \text{for} \quad \chi = \chi^L \tag{19}$$

Then, the dimensionless time $t_\star$ is taken as the heat conduction characteristic time in such a way that $Fo = 1$ and the nondimensionalized equations only depends on Bi, Γ numbers and ζ^H. Since the dimensionless derivative of the temperature $\frac{d\boldsymbol{\theta}_V}{d\zeta}$ is directly proportional to Γ (see Eq. 17 and Eq. 18) and the dimensionless heat fluxes $\nabla\boldsymbol{\theta}_V$ is inversely proportional to Bi (see Eq. 18), the two following sensitivity analyses are considered: varying Bi while maintaining Γ constant and varying Γ while maintaining Bi constant. In any case, ζ^H has been kept as constant.

In these test cases, the dimensionless numbers were evaluated with $x_\star = L$, $z_\star = H^{in}$, $T_\star = T_{ext}$, $\phi_\star = \max_{\gamma_{in}} \phi^{in}$. In addition to the nominal test case, four test cases have been defined by modifying the geometrical and physical properties of the vessel:

- in two of these test cases (denoted by $\alpha_{Bi} = 0.33$ and $\alpha_{Bi} = 3$), the vessel conductivity λ_V has been modified to increase or decrease Bi while maintaining Γ constant and $Fo = 1$.
- in the two other test cases (denoted by $\alpha_\Gamma = 0.33$ and $\alpha_\Gamma = 3$), parameter $y_\star = H^{in}$ in Eq. 16 has been modified to increase or decrease Γ while maintaining Bi constant and $Fo = 1$ (H has also been scaled accordingly to H^{in}).

These test cases, associated Bi and Γ values, characteristic times of conduction $t^x_{cond} = t_\star$ and t^z_{cond} in the radial (x-axis) and axial (z-axis) directions and modified geometrical and physical properties of the vessel are given in Table 1.

Case	Bi	Γ	t^x_{cond} (s)	t^z_{cond} (s)	λ_V (W.K^{-1}.m^{-1})	H^{in} (m)
nominal	4	2.5	1949	21650	46.86	0.06
$\alpha_{Bi} = 3$	12	2.5	1949	64960	15.62	0.06
$\alpha_{Bi} = 0.33$	1.33	2.5	643.1	7146	142	0.06
$\alpha_\Gamma = 3$	4	7.5	1949	2406	46.86	0.02
$\alpha_\Gamma = 0.33$	4	0.833	1949	194900	46.86	0.18

Table 1: Values for the pure conduction benchmark test cases

	$\epsilon_{L_2}^{\text{rel.}}$ (%)		$\epsilon_{L_1}^{\text{rel.}}$ (%)	
	$\overline{\theta}_{V,j}$	$\theta_{V,j}(x=0)$	$\overline{\psi}_{j,ext}$	$\overline{\psi}_{j,j+1}$
hybrid model ($t = 974$ s)	2.434	8.395	24.96	18.2
multi-0D model ($t = 974$ s)	22.93	33.54	56.06	not calculated
hybrid model ($t = 21650$ s)	5.305	9.937	29.06	21.71
multi-0D model ($t = 21650$ s)	31.40	43.00	108.5	not calculated

Table 2: Nominal test case

For all cases, the reference model is based on a implicit Euler scheme in time and a finite element discretization in space of Eq. 17 to Eq. 19 with a prescribed time step $\delta t = 1.0$ s, mesh sizes of $\Delta x = 0.01$ m and $\Delta z = 0.0125$ m respectively along the x-axis and the z-axis. The multi-0D and hybrid models are solving the nondimensional ODE systems based on the integral formulation of Eq. 17 to Eq. 19 with an explicit Runge-Kutta scheme (RK4) with $\delta t = 1.0$ s and mesh size $\Delta z = 0.0125$ m along the z-axis.

For all cases, the comparison between the multi-0D and hybrid models with the reference model (when necessary, 2D values are projected on the z-axis) is presented in terms of

- the relative error in L_2 norm (denoted by $\epsilon_{L_2}^{\text{rel.}}$) for the average cell temperatures $\overline{\theta}_{V,j}$ and left boundary temperatures $\theta_{V,j}(x=0)$ along the z-axis.
- the relative error in L_1 norm (denoted by $\epsilon_{L_1}^{\text{rel.}}$) for the cell upper axial heat fluxes $\overline{\psi}_{j,j+1}$ and cell right boundary heat fluxes $\overline{\psi}_{j,ext}$ along the z-axis.

Results for the nominal case at one instant of the transient ($t = t_{cond}^{x}/2$) and close to steady-state ($t = t_{cond}^{z}$) are given by Table 2. This nominal case gives a general view on the performance of the hybrid model in comparison to the multi-0D model. Other cases (increasing or decreasing the Biot and Gamma numbers) follow a seemingly monotonic trend : the smaller these numbers are, the better the results. For small values of Bi, temperature gradients *inside* the vessel are smaller (see Eq. 18) while for small values of Γ, evolution of the temperature inside the vessel is moslty due to gradient along the x-axis (see Eq. 17 and Eq. 18). For both these cases, the axial conduction plays a lesser role that explains the observed trend.

The discrepancies of the average cell temperatures $\overline{\theta}_{V,j}$ between the multi-0D and the reference models are important : at steady-state (resp. during the transient), relative errors are of 31.4% (resp. 23%) for the nominal case and can reach 58% (resp. 47%) for an increased Biot number. These discrepancies are significantly reduced by the hybrid model with a relative error of 5.3% (resp. 2.4%) and only reach a maximum value of 9.8% (resp. 4.6%) for an increased Biot number. For all cases, the same improvement is observed for the left boundary temperatures $\theta_{V,j}(x=0)$.

These improvements are made possible by the hybrid model which takes into account the axial heat fluxes $\overline{\psi}_{j,j+1}$. Modification of Bi or Γ does not seem to affect these heat fluxes (relative errors remain close to the nominal relative error of 20%).

However, for all cases, while being reduced with the hybrid model, cells right boundary heat fluxes $\overline{\psi}_{j,ext}$ errors remain important (30% for the hybrid model against 108.5% for the multi-0D model at steady state for the nominal case). While the error for the multi-0D model is associated to the neglected axial heat fluxes in the power balance, the hybrid model accuracy on

$\overline{\psi}_{j,ext}$ is actually limited by the quadratic temperature profile assumption imposed along the x-axis in each cell. Indeed, near the input heat flux ϕ^{in} discontinuity along the z-axis, taking into account the axial heat transfer lowers the average cell temperature in the heated region in such a way that the convexity of the quadratic profile (uniquely defined by the cell average temperature, the left input heat flux and the right imposed temperature, see Section 2) is modified in a non-physical way and the right boundary heat flux is underestimated. As a consequence, although this profile allows for a precise calculation of the left boundary temperature of the vessel (which can be important if ablation of the vessel is to be considered), another profile will have to be studied in future work for a better calculation of the external heat fluxes (note that this quadratic profile assumption is a common limitation for multi-OD and hybrid models and thus it is independent of the axial conduction model presented in this work).

4 APPLICATION TO IN-VESSEL MELT CORIUM RELATED CALCULATIONS

In this final Section, some calculations are shortly presented in order to highlight the use of this approximate treatment of the axial conduction for calculating the vessel wall ablation during in-vessel corium retention transients.

These calculations are based on a variation of the transient benchmarks proposed in the frame of the H2020 European project IVMR (In-Vessel Melt Retention) and further discussed in [8]. Considering an hemispherical vessel lower head (radius is 2m with a cylindrical top part of 1m-height) whose wall thickness is 15cm and initial temperature is 600K, the postulated initial corium configuration is a two-layer pool composed of a 1.5m-height oxidic pool (74wt% UO_2, 18wt% ZrO_2, 8wt% Zr) and a 10-cm thick molten steel layer. Both layers are at their liquidus temperatures (2950K for the oxidic layer, 1600K for the steel one). The associated decay heat power is 14MW. The vessel is cooled on its outside surface by water and the water saturation temperature is used for the associated Dirichlet boundary condition. The number of axial meshes for the vessel wall is 150.

For the sake of simplicity in this paper, a transient without considering the possible thermochemical interactions between the oxidic and steel layers has been calculated. As a consequence, the structure of the two-layer pool is not modified during the transient and the scope of this calculation is limited to the heat-up of the pool, the vessel wall heat-up and partial melting, the relocation of the molten steel from the wall to the top of the pool. Table 3 compares the steady-state results regarding the steel molten layer of the multi-0D and hybrid models while Figure 2 presents the heat flux and wall thickness profiles at $t = 12100$s, close to steady-state.

In [9], 2D stationary conduction calculations for the vessel wall were performed based on imposed heat flux profiles associated with two-layer pool configurations extracted from severe accident scenario calculations for the APR1400 reactor. While the ablation transient was not calculated, an element-birth-and-death technique was used to take into account the vessel wall thickness change. In this work, without feedback of the vessel calculation onto the pool mass and energy balance, the maximum heat flux at the focusing region was decreased by 10% to 20% when considering the 2D heat conduction in the vessel wall.

Table 3: Molten steel layer associated quantities at steady-state

	$m_{\text{steel}}^{\text{ablated}}$ (t)	h_{steel} (cm)	P_{steel}^{lat} (MW)	$\phi_{\text{steel}}^{lat}$ (MW.m^{-2})
multi-0D model	8.795	20.48	4.832	1.878
hybrid model	8.731 (-0.73%)	20.41 (-0.34%)	4.830 (-0.04%)	1.883 (+0.27%)

$m_{\text{steel}}^{\text{ablated}}$ mass of molten steel form the vessel wall
h_{steel} height of the molten steel layer
P_{steel}^{lat} power that is transmitted from the molten steel layer to the vessel wall
$\phi_{\text{steel}}^{lat}$ average heat flux imposed by the molten steel layer to the vessel wall

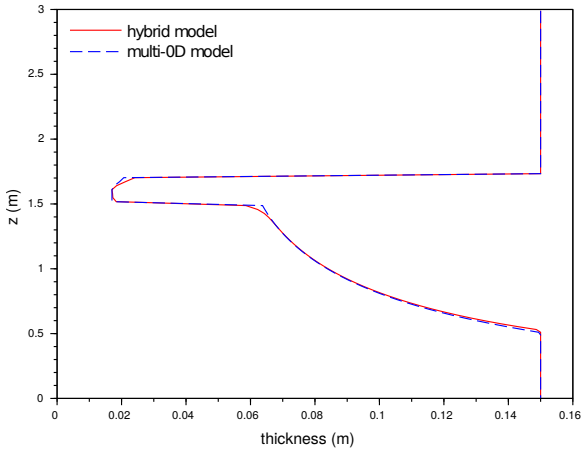

(a) Wall thickness as a function of z

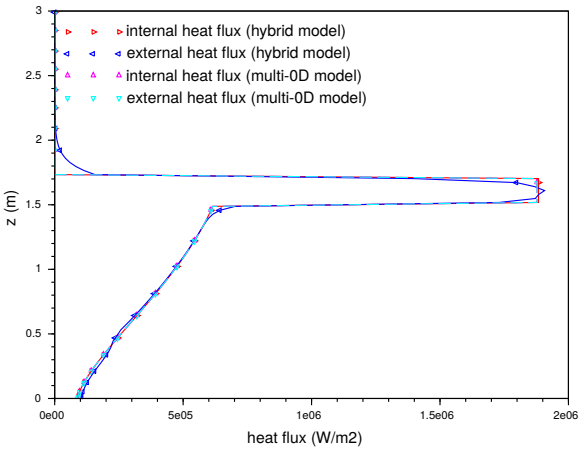

(b) Internal and external heat fluxes as a function of z

Figure 2: Vessel associated quantities at steady-state ($t = 12100$s) for both the multi-0D and hybrid wall models

We can hope that the vessel ablation is more precisely calculated by the hybrid model since discrepancies of the left boundary temperature of the vessel wall are reduced with this model in comparison to the multi-0D model (see Section 3). For the considered case of corium pool stratification, it seems that the axial conduction in the vessel wall has only little impact on the vessel ablation (-0.73% at steady state of vessel mass ablated added to the corium pool).

The hybrid model allows for a better calculation of the external heat flux : more heat is removed from the vessel wall in region on top of the corium pool ($z >= 1.7$ in Figure 2b) due to conduction heat transfer from the high-heat-flux region ($1.4 < z < 1.7$) corresponding to the molten steel layer of the corium pool. However, considering the axial conduction in the high-heat-flux region seems to go against the quadratic profile assumption (in particular on the right boundary - it is the same scenario as in Section 3) leading to external heat fluxes only poorly calculated (it should not be higher than the imposed internal heat flux). This explains why the maximum heat fluxes at the focusing region were not reduced in our work (in comparison to calculations found in [9]). This does not invalidate the proposed axial conduction model but encourages us to couple it with a more accurate temperature model in this region (other temperature models are proposed in [10] for example).

5 CONCLUSION

Within the framework of Severe Accident studies for Light Water Reactors (LWRs), in-vessel corium behavior and associated risk of vessel failure are matters of prime interest. In the

frame of the PROCOR software platform development [4], the vessel wall discretized by 1D axial meshing was treated in crude way by neglecting the axial conduction as in [6] in such a way that the one-phase Stefan problems associated with the different meshes are decoupled.

In this paper, an improvement of the vessel wall conduction model is proposed by taking into account the axial conduction. In Section 3, test cases without ablation (based on a typical in-vessel configuration) have shown that, in comparison to a 2D conduction model solved with finite elements taken as reference, the proposed hybrid model allows us to greatly reduced discrepancies in terms of average temperature and boundary temperature of the vessel wall. However, these test cases have also highlighted a pathology associated with the temperature model used in each mesh leading to imprecise calculation of the heat fluxes at the external vessel wall.

In Section 4, this pathology has been found again in the high-heat-flux region of the vessel wall on an in-vessel corium transient calculation under IVR conditions. This does not invalidate the proposed axial conduction model but encourages us to adapt, in future work, the temperature model in this region (other temperature models are proposed in [10] for example).

ACKNOWLEDGMENTS

This work has been carried out within the framework of the PROCOR platform development funded by CEA, EDF and AREVA.

REFERENCES

[1] J. L. Rempe, D. L. Knudson, M. Cebull, and C. L. Atwood. Potential for in-vessel retention through ex- vessel flooding. In *Proc. of the OECD/CSNI Workshop on In-Vessel Core Debris Retention and Coolability*, 1998.

[2] T. G. Theofanous, C. Liu, S. Addition, S. Angelini, O. Kymalainen, and T. Salimassi. In-vessel coolability and retention of a core melt. *Nuclear Engineering and Design*, 169:1–48, 1997.

[3] Henry Hu and Stavros A Argyropoulos. Mathematical modelling of solidification and melting: a review. *Modelling and Simulation in Materials Science and Engineering*, 4(4):371–396, July 1996.

[4] R. Le Tellier, L. Saas, and F. Payot. Phenomenological analyses of corium propagation in LWRs: the PROCOR software platform. In vai, editor, *Proc. of the 7th European Review Meeting on Severe Accident Research ERMSAR-2015*, Marseille, France, 2015.

[5] R. Le Tellier, L. Saas, and S. Bajard. Transient stratification modelling of a corium pool in a LWR vessel lower head. *Nuclear Engineering and Design*, 287:68–77, 2015.

[6] B. Tourniaire, B. Spindler, G. Ratel, J. M. Seiler, B. Iooss, M. Marquès, F. Gaudier, and G. Greffier. "the LEONAR code: a new tool for PSA level 2 analyses". In *Proc. of Joint OECD/NEA - EC/SARNET2 Workshop on In-Vessel Coolability*, volume NEA/CSNI/R(2010)11, p. 105-121, 2009.

[7] R. Le Tellier, E. Skrzypek, and L. Saas. On the treatment of plane fusion front in lumped parameter thermal models with convection. *Applied Thermal Engineering*, 120:314–326, 2017.

[8] L. Carénini, F. Fichot, N. Bakouta, R. Le Tellier, L. Viot, I. Melnikov, P. Pandazis, and A. Filippov. Main outcomes from the ivr code benchmark performed in the IVMR project. In *Proc. of the 9th European Review Meeting on Severe Accident Research ERMSAR2019*, Prague, Czech Republic, 2019.

[9] Jaehoon Jung, Sang Mo An, Kwang Soon Ha, and Hwan Yeol Kim. Evaluation of heat-flux distribution at the inner and outer reactor vessel walls under the in-vessel retention through external reactor vessel cooling condition. *Nuclear Engineering and Technology*, 47(1):66 – 73, 2015.

[10] T.G. Myers. Optimal exponent heat balance and refined integral methods applied to stefan problems. *International Journal of Heat and Mass Transfer*, 53(5):1119 – 1127, 2010.